JESK J Ergon Soc Korea 2016; 35(5): 319-341
http://dx.doi.org/10.5143/JESK.2016.35.5.319
http://jesk.or.kr eISSN:2093-8462

Analysis of Lower-Limb Motion during Walking on Various Types of Terrain in Daily Life

Myeongkyu Kim, Donghun Lee

Mechanical Engineering, Soongsil University, Seoul, 06978

Corresponding Author
Donghun Lee
Mechanical Engineering, Soongsil University, Seoul, 06978
Mobile : +82-10-3703-9686
Email : dhlee04@ssu.ac.kr

Received : April 19, 2016
Revised : May 15, 2016
Accepted : September 19, 2016

Objective: This research analyzed the lower-limb motion in kinetic and kinematic way while walking on various terrains to develop Foot-Ground Contact Detection (FGCD) algorithm using the Inertial Measurement Unit (IMU).

Background: To estimate the location of human in GPS-denied environments, it is well known that the lower-limb kinematics based on IMU sensors, and pressure insoles are very useful. IMU is mainly used to solve the lower-limb kinematics, and pressure insole are mainly used to detect the foot-ground contacts in stance phase. However, the use of multiple sensors are not desirable in most cases. Therefore, only IMU based FGCD can be an efficient method.

Method: Orientation and acceleration of lower-limb of 10 participants were measured using IMU while walking on flat ground, ascending and descending slope and stairs. And the inertial information showing significant changes at the Heel strike (HS), Full contact (FC), Heel off (HO) and Toe off (TO) was analyzed.

Results: The results confirm that pitch angle, rate of pitch angle of foot and shank, and acceleration in x, z directions of the foot are useful in detecting the four different contacts in five different walking terrain.

Conclusion: IMU based FGCD Algorithm considering all walking terrain possible in daily life was successfully developed based on all IMU output signals showing significant changes at the four steps of stance phase.

Application: The information of the contact between foot and ground can be used for solving lower-limb kinematics to estimating an individual's location and walking speed.

Keywords: Foot-ground contact, Lower limb, Gait analysis, Inertial measurement unit, Walking terrain

1. Introduction

Mobile internet-enabled devices, global positioning system (GPS), and cellular communication networks are successfully employed to provide location tracking services of human for various purposes such as children and customer tracking, etc. In certain fields of human robot interaction (HRI), the accurate positioning of a human in real-time is also needed to guarantee desirable robot behaviors. Recently, a number of studies were carried out for localization under various GPS-denied (Ng et al., 2004; Hogg et al., 2002) and vision system-denied (Shimizu et al., 2012; Morioka et al., 2004)

environments. Seco et al. (2009) estimated the trajectory of pedestrians through a proposed step detection algorithm and stride length estimation algorithm using IMU sensors attached to the top of the foot. However, it is reported that a positioning error of less than 5% occurs according to the pedestrians' walking patterns. Yuan and Chen (2012; 2014) estimated the location of pedestrians within a positioning error of less than 2% by using lower-limb kinematics. Yuan and Chen also developed a new force sensitive resistor (FSR)-array insole because the detection of the stance phase must be carried out prior to calculating the position of a specific point on the pelvis by solving the lower-limb kinematics. For FGCD, Yuan and Chen also installed the developed FSR-array insole at the bottom of the shoes; the stationary ankle was defined as a reference point for solving the lower limb kinematics (Eng and Winter, 1995) and differential kinematics.

Previously, pressure sensors attached at the bottom of shoes was used to detect the contacts between the foot and ground. Ahn et al. (2004) showed successful gait phase detection by using a FSR-gyro sensor system for detection of the initial contact, flat foot, heel off, and swing phases, and using a tilt sensor system for detection of the initial contact, 1st tibia vertical, foot off, and 2nd tibia vertical. In addition, Pappas et al. (2004) used FSRs (Interlink El. Inc., 152NS) and a gyro (Murat, ENC-03JA) to detect the stance, heel off, swing, and heel strikes. After careful consideration of the above research, as well as other research regarding the lower limb (Benocci et al., 2009; Bamberg et al., 2008; Chen et al., 2009), it is confirmed that the shoe force plates and FSR-array insoles were mainly used to detect the stance phase and foot-ground contacts.

However, the shoe force plates and FSR-array insoles can be considered as additional sensors to the IMU based human localizations. Moreover, the shoe force plates and insoles have some disadvantages of complex connections with the data logger, robustness for repetitive load (D'Attanasio et al., 2001), and sensitivity in regard to the foot size of the subjects (Pappas et al., 2001). That is, the IMU sensors are crucial for estimating the location of the pedestrian because the inertial information of the lower-limbs is essential to solve the lower-limb kinematics.

Accordingly, if the FGCD can be successfully conducted by using only IMU sensors, it can be expected that the connections between sensors and the data acquisition (DAQ) device, as well as convenience in sensor installations will be greatly improved. Bergmann et al. (2010) have tried to detect the foot-ground contact while descending stairs using IMU on the thigh, shank and foot, and also estimate the velocity of the pelvis and trajectory of foot by using lower-limb kinematics with an error by 0.04±0.03s. Ferrari et al. (2015) developed the algorithm for detecting foot off and initial contact using IMU on foot. Based on the algorithm, a mobile solution for estimating the stride duration, length and velocity at various walking speeds were suggested. Salarian et al. (2013) developed the algorithm for detecting initial contact and terminal contact by using angular velocity of gyro on the shank. Only using two gyros, stride-length and stride-velocity were estimated with error by 3.8±6.6cm and 3.8±5.6cm/s. In that study, the error of stride-length and stride-velocity was -0.8±6.6cm and -0.4±5.3cm/s when using four gyros. The number of gyro was also reduced by half with relatively small impact on accuracy. But it should be noted that these previous researches on IMU or gyro based foot-ground contact detection have been successfully conducted, but were only available at the flat ground or stair descent.

It is definitely logical to assume that the IMU based FGCD will be influenced by the walking terrain as well as walking speed, walking patterns, and gender. Chen et al. (2009) proposed a fuzzy logic classifier that can separately detect the type of walking, flat walking, descending stairs, and ascending stairs by using an IMU sensor. Kim and Lee (2016) developed an IMU based FGCD algorithm that can successfully detect stance phase on the flat ground, stairs and slope when the pedestrian is walking at various walking speeds. IMUs are mounted on the pelvis, shank and foot of the participant. Heel strike, full contact, heel off and toe off, the four steps of stance phase, were detected by using the kinetic and kinematic parameters of shank and foot. In case of toe off on the stairs ascent, however, time delay of 60ms was observed. Li et al. (2012) and Li and Wang (2012) also proposed a robust algorithm to track the moving trajectory in walking and walking-running combined motions as well as running by using an IMU installed at the front surface of a boot. Dadashi et al. (2014) measured six clearance parameters of 239 male and 315 female subjects aged 60 to 70 by using an IMU installed on the top of the foot. The six clearance parameters included 1) heel strike pitch angle, 2)

maximum heel clearance, 3) first local maximum of the toe clearance, 4) second local maximum of the toe clearance, 5) minimum of the toe clearance, and 6) velocity of foot at minimum toe clearance. Moreover, through an ANOVA test, it was confirmed that all clearance parameters except for minimum toe clearance are affected by gender. However, the heel strike pitch angle was the only parameter related to the FGCD.

Unfortunately, few studies have been conducted on the IMU based FGCD according to the variations of walking terrain, walking speed, walking patterns, and gender. Accordingly, this research involves a feasibility study aimed at developing an FGCD algorithm in various terrain that we encounter in everyday life using only IMU sensors. This research is a preceding study of development of an IMU based FGCD algorithm (Kim and Lee, 2016) which can overcome uncontrollable factors such as walking terrains and walking speed. In addition, this research is believed to be a worthwhile investigation for accumulating knowledge on the lower-limb motions in aspect of the FGCD.

In this research, to realize an IMU based FGCD algorithm for flat ground, slope and stairs, all IMU outputs showing significant changes on the moments of the four different foot-ground contacts will be carefully identified through walking experiments in five terrains. The foot-ground contact phases are composed of heel strike (HS), full contact (FC), heel off (HO), and toe off (TO). The walking terrains for experiments are composed of flat ground as well as up and down a slope and stairs. The first hypothesis of this research is that HS, FC, HO, and TO on every terrain encountered in daily life can be independently detected by using IMU sensors' outputs. The results of benchmark study using the wireless FSR-array showed that the other sensors used for the FGCD can be successfully removed from the current sensor system (Yuan and Chen, 2014). This method was originally supposed to be apply in military applications such as pedestrian position tracking in the GPS-denied environment. Hence the major target for this research is adult male. In section 2, all information on subjects, measurement systems, and analysis methodology are described. In section 3, all experimental results from walking on the flat ground, as well as up and down a slope and stairs are carefully analyzed in terms of the acceleration and orientation of the lower-limb segments. In section 4, the walking terrain specific gait characteristics are described in terms of the four different contact phases. To validate the feasibilities of the IMU-based foot-ground contact detection with some threshold-based criterions, the benchmark study using the wireless FSR-array insole is also performed.

2. Method

2.1 Participants

In this research, 10 adult participants (Age: 25.5±0.85 years; Height: 176.2±5.88cm; Weight: 68.6±7.60kg; Gender: male) who had not suffered from any type of musculoskeletal disorder participated in all five independent gait experiments on flat ground, as well as up and down a slope and stairs. As a preceding research for developing an IMU based FGCD algorithm (Kim and Lee, 2016) which can be used on various terrains with various walking speed, the feasibility was examined for the case of adult male. Informed consent was obtained from each qualified participant prior to his participation in the research. Before starting the main experiments, gait training on the different terrains was carefully performed to familiarize the participants with the 5-IMU attached to their body.

2.2 Measurements system

As shown in Figure 1, the 5-IMU (MTx, XSENS) was attached to the feet, shanks, and pelvis to determine the three-dimensional accelerations, orientations, and angular velocity of each body segment during the gait experiments. The two sensors in the 5-IMU were mounted on the right and left shanks instead of on the calf to minimize the effect of contraction and relaxation of the muscles as shown in Figure 1. Each IMU was firmly fixed to the appointed segments using straps. Instead of the inertial coordinate frame that was fixed on the Earth, a new virtual reference coordinate frame (the body-fixed coordinate frame, $\{B_f\}$), was attached to the participant's body as shown in Figure 1. $\{B_f\}$ is on the lines of intersection of three anatomical planes. That is, the most important

criterion in the experiments (which involved several participants), was the measurements of the lower-limb motions of all participants on the same reference coordinate frames. Thus, $\{B_f\}$, $[x_{Bf}, y_{Bf}, z_{Bf}]^T$, shown in Figure 1 were created by using an IMU mounted on the back of the pelvis.

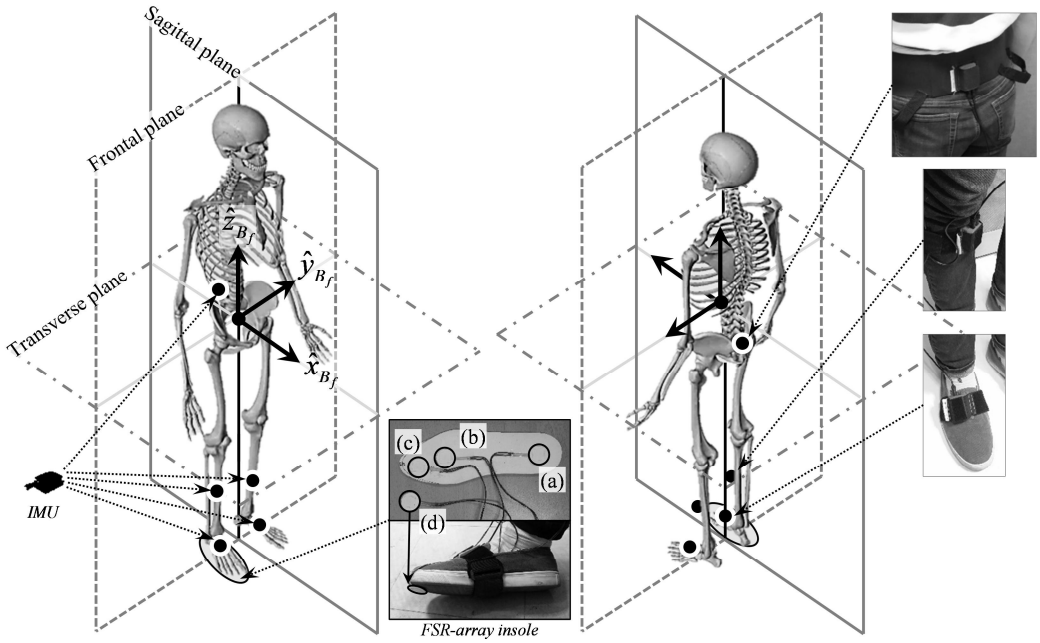

Figure 1. Three principle planes for describing gait analysis, body-fixed coordinate frame as a common reference coordinate frame of inertial measurement unit output signals, positions of inertial measurement unit mounted on body segments, position of force sensitive resistor system for benchmark study, and positions of four force sensitive resistor installed on insole and shoe: (a) heel, (b) metatarsophalangeal joint, (c) toe and (d) shoe tip

To create $\{B_f\}$ before starting walking, orientations of the sensor-fixed coordinate frame of pelvic IMU should be recorded while the participants change their postures from standing postures ($\{S_{f.pelvis.stand}\}$) to stooping postures ($\{S_{f.pelvis.stoop}\}$). That is, $\{S_{f.pelvis.stand}\}$ will be coincident with the $\{S_{f.pelvis.stoop}\}$ by being rotated about the vector k by an angle θ according to the right-hand rule. Then, the rotation vector k can be obtained by following using equivalent angle-axis representation (John, 2005). z_{Bf} is an unit vector heading the opposite direction of gravity. x_{Bf} is obtained by the cross product of k and z_{Bf}, and y_{Bf} is also obtained by the cross product of z_{Bf} and x_{Bf}.

Because the orientations of each sensor-fixed frame ($\{S_j\}$, j = right and left foot and shank) of IMU are different, the orientation compensation unifying the orientations of each $\{S_{fj}\}$ should be processed. Each compensated sensor-fixed coordinate frames ($\{C_{Sfj}\}$) are defined by orientation compensations which are same with the differences between $\{S_{fj}\}$ and $\{B_f\}$ when the posture of participant

$$\underbrace{{}^{S_{f.j.0}}R_{C_{S_{f.j}}}}_{\substack{\text{Orientation of } \{C_{S_{f.j}}\} \text{ expressed in} \\ \{S_{f.j}\} \text{ when straight aligned}}} = \overbrace{{}^{S_{f.j.0}}R_{G}}^{\substack{\text{Orientation of global frame expressed in} \\ \{S_{f.j}\} \text{ when straight aligned}}} \square \underbrace{{}^{G}R_{B_f}}_{\substack{\text{Orientation of } \{B_f\} \\ \text{expressed in grobal frame}}} \quad (1)$$

is standing. The orientations of $\{S_{fj}\}$ expressed in $\{C_{Sfj}\}$ when straight aligned are obtained by using the orientation of $\{B_f\}$ and initial orientations of $\{S_{fj}\}$.

The changes of the orientations of $\{C_{Sfj}\}$ are same with the changes of the posture of lower-limb segments when the participant moves. The procedure to calculate the orientations of $\{C_{Sfj}\}$ expressed in $\{B_f\}$ is as follows: the orientations of $\{S_{fj}\}$ expressed in global frame, IMU output, are expressed by $\{B_f\}$, and multiplied by the orientation compensation.

$$\underbrace{{}^{B_f}R_{C_{S_{f\cdot j}}}}_{\substack{\text{Orientation of } \{C_{s_{f\cdot j}}\} \\ \text{expressed in } \{B_f\}}} = \overbrace{{}^{B_f}R_{G}}^{\substack{\text{Orientation of global frame} \\ \text{expressed in } \{B_f\}}} \; \underbrace{{}^{G}R_{S_{f\cdot j}}}_{\substack{\text{Orientation of } \{S_f\} \text{ expressed in} \\ \text{global frame (IMU output)}}} \; \overbrace{{}^{S_{f\cdot j\cdot 0}}R_{C_{s_{f\cdot j}}}}^{\text{Orientation compensation}} \tag{2}$$

Also, the orientations of $\{C_{Sfj}\}$ are same with $\{B_f\}$ when the participant is standing posture.

$$\underbrace{{}^{B_f}R_{C_{S_{f\cdot j\cdot 0}}}}_{\substack{\text{Orientation of } \{C_{S_{f\cdot j}}\} \text{ expressed in} \\ \{B_f\} \text{ when straight aligned}}} = I \tag{3}$$

More detailed explanations about the IMU installation and the coordinate frames are described in section "Design of FGCD algorithm and issues on IMU sensor installations".

The sampling rate of each IMU was set to 50Hz, which is the maximum sampling rate for simultaneous usage of the 5-IMU with wireless. The maximum sampling rate of 5-IMU is 200Hz when the IMU is tethered, however the space for gait experiments are relatively wide (flat ground and slope: 10m, stairs: 15 step) to use tethered. Which is the reason why the IMU was used as wireless. The collected accelerations, orientations, and angular velocity from IMUs were post-processed by the MATLAB. Through the post-processing, the data expressed in the sensor-fixed coordinate frames can be transformed to the data expressed in the $\{B_f\}$, as mentioned earlier.

While all participants wearing IMUs were walking on predetermined walking terrains. The participant's motions were record in the sagittal plane by using video camera at 60 frames per seconds. Every moments of the HS, FC, HO, and TO (Figure 2) were

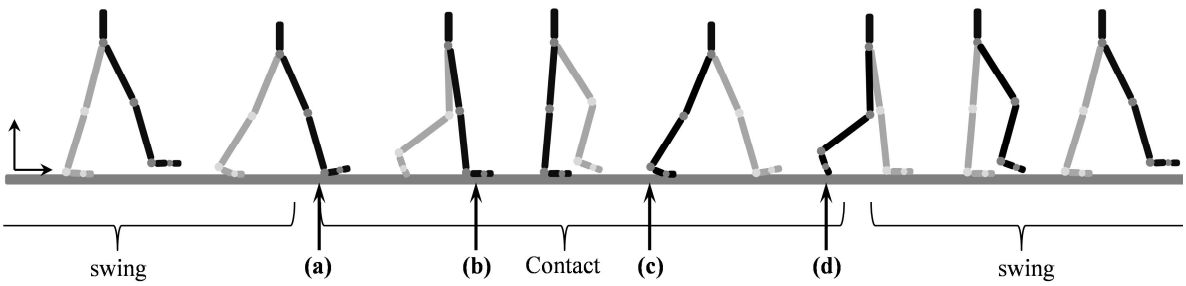

Figure 2. Four steps of the contact phase during the gait experiment: (a) heel strike, (b) full contact, (c) heel off, and (d) toe off. One leg is in its swing phase, while the other leg is in its contact phase with the ground

discovered by carefully watching the recorded video in low speed mode. And, at each moment of foot-ground contact, the sensor data of the three-dimensional accelerations and orientations expressed in the $\{B_f\}$ were examined.

After developing the IMU based FGCD algorithm, the wireless FSR (A401-25, TECSCAN) -array insole was used for validating the performance of proposed FGCD algorithm. As shown in Figure 1, 4-FSR are installed on the heel, metatarsophalangeal joint (MT), toe and shoe tip (ST) to confirm the moments of HS, FC, HO and TO. The sampling rate of FSR and IMU were synchronized (50Hz) to prevent possible jitters in numerical processing.

2.3 Design of experiments

The walking speed on flat ground was determined to be 1.49m/s, which is known as the statistically average speed of a man in his twenties to thirties (Park et al., 2007). In regard to walking up and down a set of stairs, with a 15cm riser and 35cm tread, the speeds were determined to be 0.67m/s for ascending and 1.01m/s for descending the stairs by referring to the statistically average speeds of a man under the age of thirty (Choi and Hong, 2013). In regard to walking up and down the slope, the speeds were determined to be 1.31m/s for ascending and 1.40m/s for descending the slope, with consideration of the average speed of 10 participants as estimated in our preliminary experiments.

In order to assist participants in maintaining the walking speeds mentioned above, a metronome was adopted in the experiments. In the cases of walking along the level ground and the slope, the metronome helped the participants to match their pace to the beats of the metronome. However, due to the difficulty involved in ascending and descending stairs, the device is only used to assist the participant to make HS for ascending or Toe Strike (TS) for descending stairs. However, unnatural lower-limb motions can be generated by keeping pace with the predefined walking speed. In order to avoid it, participants were asked to walk naturally and smoothly. As results from gait experimental video, the slight difference of walking speed between predefined walking speed and actual walking speed of participants were observed -1% to 5% for flat ground, -0.7% to 0.6% for stairs, and -3% to 6% for slope.

3. The Experimental Results

One hundred trials, corresponding to 10 participants times 2 trials for 5 walking terrain, were correctly collected.

The accelerations measured from the IMU typically include the gravitational acceleration of -9.81m/s^2 in the z-direction of the inertial coordinate frame. Gravity compensation should be made in the accelerometer measurements in order to obtain exact observations of reaction forces in the z-direction (Nistler and Selekwa, 2011).

Before discussing the main experimental results, it should be noted that all IMU outputs are expressed in the $\{B_f\}$ shown in Figure 1. In addition, we will focus on the accelerations in the x and z axes because the acceleration in the y-axis does not show significant change in FGCD. In other words, the magnitude range ay of the foot is from -12.39 to 10.14m/s^2 while walking on the flat ground or up and down the slope and stairs, while the a_x and a_z of the foot range from -54.1 to 60.2m/s^2 and from -42.6 to 33.0m/s^2, respectively. The magnitudes of accelerations of the shanks were too small to find any significant differences between the moment of contact and the swing phase. The a_x, a_y, and a_z range from -21.1 to 25.6m/s^2, from -12.16 to 11.89m/s^2, and from -9.04 to 18.92m/s^2, respectively. However, the pitch angle β (which is the rotation angle about the y-axis) represents significant change at the moments of the foot-ground contact phases, and ranges from -43.4 to 66.2 *degrees*. Figure 3 presents the plots of the accelerations and orientations of the shanks and feet while the participant was walking on flat ground. In addition, it is confirmed that the patterns and amplitudes of the signals in these plots are quite similar to the results from the other terrains, which is why we can only focus on a_x and a_z for the foot and β for both the foot and the shank.

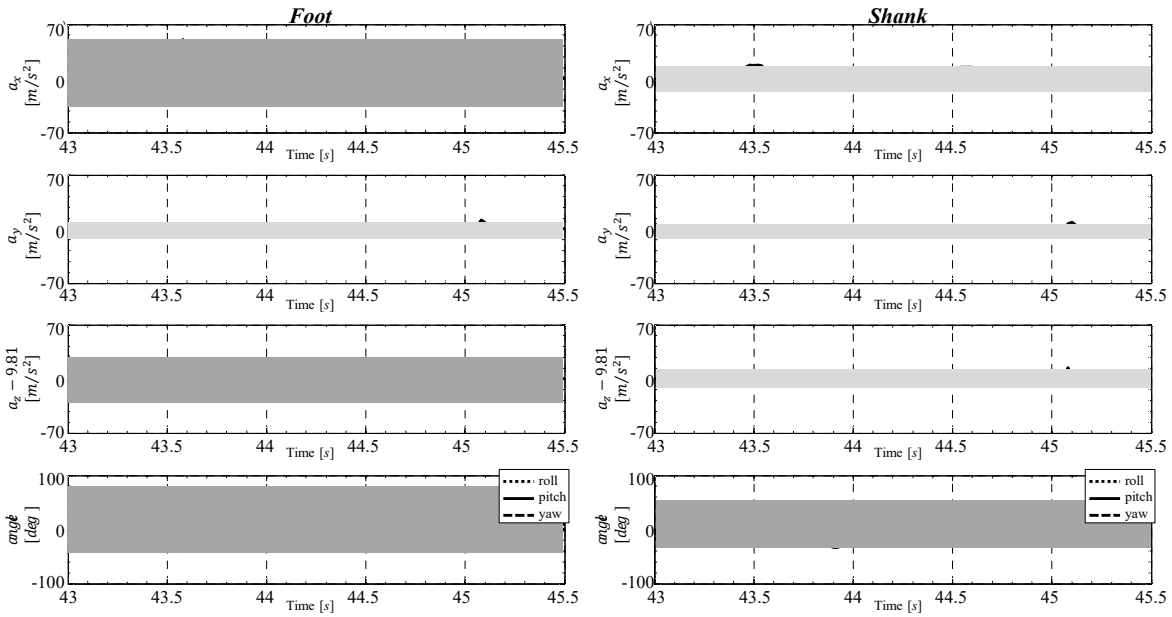

Figure 3. Accelerations and orientations of the feet and shanks while walking on flat ground. Foot: -54.1m/s^2 ≤ a_x ≤ 60.2m/s^2, -12.39m/s^2 ≤ a_y ≤ 10.14m/s^2, -42.6m/s^2 ≤ a_z -9.81m/s^2 ≤ 33.0m/s^2 and -42.9° ≤ β ≤ 81.1°. Shank: -21.09m/s^2 ≤ a_x ≤ 25.6m/s^2, -12.16m/s^2 ≤ a_y ≤ 11.89m/s^2, -9.04m/s^2 ≤ a_z -9.81m/s^2 ≤ 18.92m/s^2 and -34.4° ≤ β ≤ 66.2°

Table 1 presents the experimental results of the mean and standard deviations of the acceleration of the foot in x_{Bf} direction (a_x), acceleration of the foot in z_{Bf} direction (a_z), pitch angle of the foot (β_f), rate of pitch angle of the foot ($\dot{\beta}_f$), pitch angle of the shank (β_s) and rate of pitch angle of the shank ($\dot{\beta}_s$) at the moment of HS, FC, HO and TO for the five different walking terrain.

In the following sections, the lower-limb motion analysis for walking on the five different terrains are carefully performed to examine tendencies and correlations among six main parameters measured from IMU sensors. And then, the results will be carefully discussed to examine the feasibilities of the IMU-based FGCD algorithm.

Table 1. Mean and standard deviations of the accelerations, pitch angle, and rate of pitch angle of the foot and shank

Case			Heel strike (Toe strike for stair descent)		Full contact		Heel off		Toe off	
			Mean	S.D.	Mean	S.D.	Mean	S.D.	Mean	S.D.
Level road	Foot	a_x	-35.6	7.67	-0.56	0.51	1.34	0.68	44.8	5.55
		a_z	-34.8	4.85	0.74	0.49	-0.05	0.45	5.43	10.2
		β_f	-25.8	6.24	-1.32	1.87	11.5	0.59	72.2	4.51
		$\dot{\beta}_f$	-0.92	1.51	0.32	0.20	2.30	0.52	2.43	2.48
	Shank	β_s	-29.5	2.75	-7.71	4.37	14.1	3.92	49.8	4.48
		$\dot{\beta}_s$	0.27	0.81	1.77	0.29	2.45	0.47	1.53	0.88

Table 1. Mean and standard deviations of the accelerations, pitch angle, and rate of pitch angle of the foot and shank (Continued)

Case			Heel strike (Toe strike for stair descent)		Full contact		Heel off		Toe off	
			Mean	S.D.	Mean	S.D.	Mean	S.D.	Mean	S.D.
Stair ascent	Foot	a_x	-18.2	1.84	-0.59	1.02	1.76	0.75	10.4	3.70
		a_z	-5.64	1.87	0.29	0.42	-0.14	0.22	14.4	10.3
		β_f	-1.91	4.38	-1.05	1.79	8.91	2.01	48.0	7.59
		$\dot{\beta}_f$	-1.23	0.79	-0.16	0.11	2.62	0.81	2.49	1.27
	Shank	β_s	13.3	3.83	15.5	3.44	10.8	3.86	32.3	9.77
		$\dot{\beta}_s$	-1.59	0.57	0.06	0.16	1.07	0.61	3.33	0.87
Stair descent	Foot	a_x	-33.1	6.02	0.54	1.73	3.26	1.45	42.7	5.19
		a_z	-9.73	5.00	-0.32	0.96	-0.19	0.82	1.99	5.37
		β_f	16.9	5.04	2.12	3.41	10.7	1.01	52.3	4.11
		$\dot{\beta}_f$	-0.12	0.97	0.01	0.36	2.57	1.14	-0.23	1.39
	Shank	β_s	-7.78	2.13	11.0	3.15	37.4	6.70	54.2	3.66
		$\dot{\beta}_s$	-1.46	0.55	2.10	0.60	2.94	0.52	-0.68	1.21
Slope ascent	Foot	a_x	-30.0	3.50	-0.58	0.22	1.72	0.65	44.1	6.29
		a_z	-19.8	5.20	0.70	0.66	-0.13	0.24	12.6	7.10
		β_f	-23.0	3.49	-12.3	2.87	-0.04	1.33	66.8	4.93
		$\dot{\beta}_f$	-1.40	0.81	0.13	0.17	2.52	0.83	2.37	1.39
	Shank	β_s	-17.7	2.74	-1.76	3.05	10.8	3.12	35.2	4.97
		$\dot{\beta}_s$	-0.65	0.75	1.33	0.29	1.44	0.45	1.76	0.80
Slope descent	Foot	a_x	-33.8	3.50	-0.55	0.44	1.85	1.16	47.1	7.24
		a_z	-25.9	7.07	0.77	0.57	-0.79	0.68	3.15	11.5
		β_f	-22.2	6.43	8.19	2.26	18.5	1.19	70.1	9.21
		$\dot{\beta}_f$	-1.30	0.98	0.29	0.36	2.51	0.87	2.17	2.15
	Shank	β_s	-19.0	3.68	5.15	3.99	34.5	8.88	61.9	4.02
		$\dot{\beta}_s$	-0.06	0.79	2.69	0.70	2.75	0.75	1.55	0.84

† The number of participants is 10.
‡ Unit: acceleration in m/s^2, pitch angle β in *degrees*, pitch rate $\dot{\beta}$ in rad/s.

3.1 Experiment 1: Walking on the flat ground

During the swing phase (shown in Figure 4, Section I), the positive peak values of the pitch angle of the foot (72.2±4.51°) and the shank (49.7±4.43°) are gradually decreased to the negative peak values (foot: -25.7±6.20°, shank: -29.88±2.74°) according to the change from hyperextension to flexion of the hip, flexion to extension of the knee, and the plantar flexion to dorsiflexion of the ankle. a_x, acceleration in the walking direction, reaches its positive peak values (45.4±6.74m/s^2) immediately after the TO and

gradually decreases to its negative peak values (-35.5±7.78m/s^2) at the moment of HS. The v_x of the foot is increased until the middle of the swing phase and is decreased immediately before the HS; it can be confirmed that the velocity of the heel reaches zero consistently with the HS. The validity of the analysis and the decision on the movement of the HS can be given by the result whereby the pitch angle of the foot decreased to its negative peak values (-25.7±6.20°). As the foot approaches the ground during the swing phase, a_z is gradually decreased from a positive value to a negative peak value until the HS, as shown in Figure 4 above. In addition, as the foot rises from the ground during the swing phase, a_z shows a tendency to increase from a negative value to a positive value overall; however, it is worth noting that a_z sharply decreases from a positive to a negative value shortly after the TO. In this case, the vertical position of the foot is lowered slightly after TO, and then rises again; that is, from the moment of the TO to the HS, a_z shows a tendency to fluctuate between negative and positive values.

In Figure 4, Section II, the stance phase starts from the moment of the HS. At this time, the flexion of the hip and dorsiflexion of the ankle are reduced and extension of the knee is maintained. Because of the downward rotation of the tip of the foot around the heel as an axis of rotation, the pitch angle of the foot (-25.7±6.20°) and the shank (-29.9±2.74°) (in their negative peak values) increases to 0°.

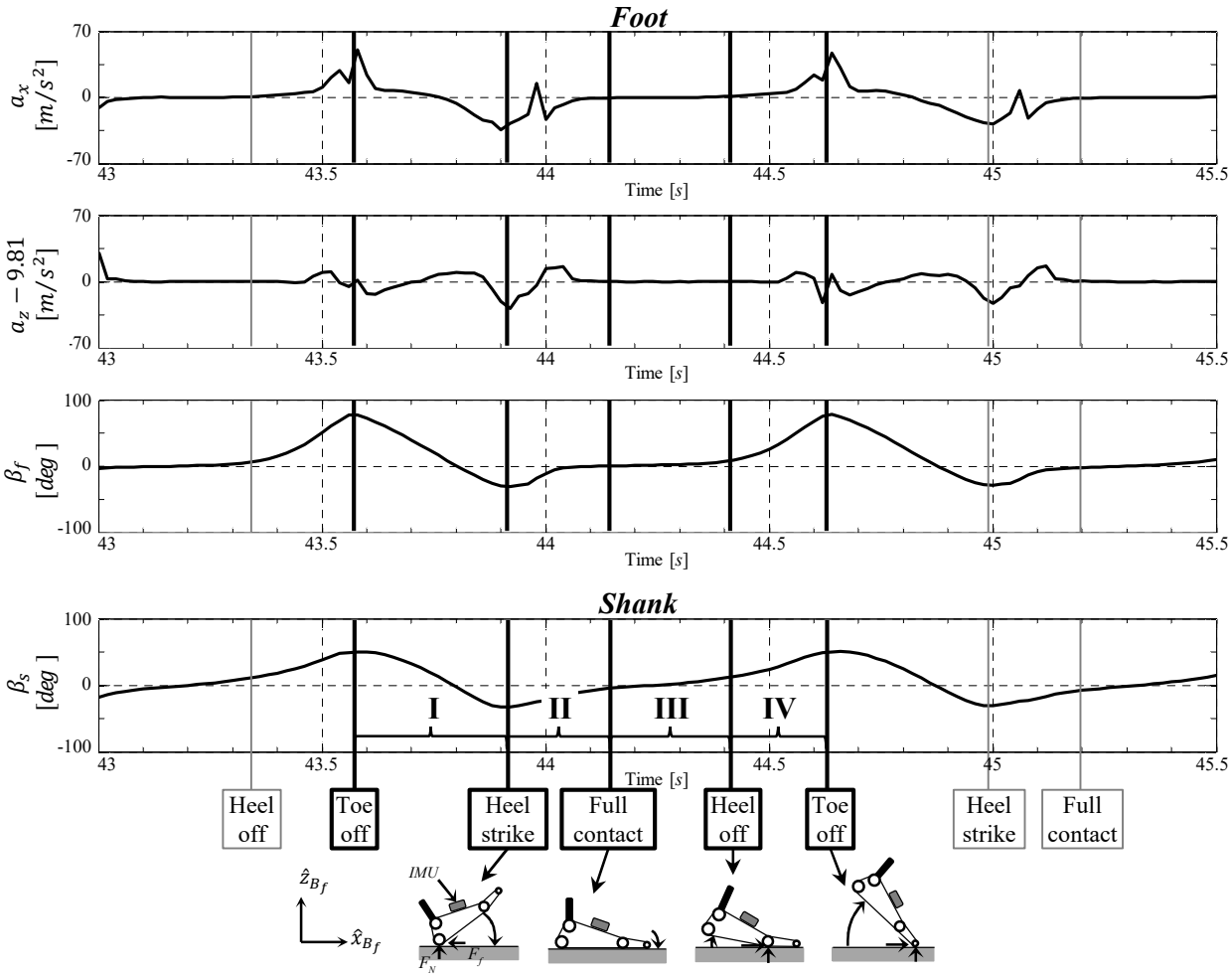

Figure 4. Accelerations and orientation of foot and shank in sagittal plane while walking on flat ground; time intervals of all sections are as follows: 0.4s for I, 0.18s for II, 0.34s for III, and 0.2s for IV

The gradual decrease of the a_x to its negative peak value (-35.5±7.78m/s^2) is commonly observed in every contact between the heel and the ground. Moreover, it results from the friction force in the negative x direction. After the sharp increase followed by its negative peak value (-33.8±5.54m/s^2) at the HS, a_z changes to its positive (peak) value due to the effect of reaction forces from the ground to the heel.

While a_x, a_z, and all orientation angles of the foot are maintained at around 0 during the FC, it is confirmed that the shank's pitch angle is gradually increased from a negative value to a positive value. When the ankle is fixed on the ground during the FC, it is used as an axis of rotation that allows the pelvis to move forward as if it is in an inverted pendulum motion. For this stance phase, the plantar flexion of the ankle is converted to the dorsiflexion, the extension of the knee is maintained, and the flexion of the hip is converted to hyperextension. As a result, the pitch angle of the shank can be gradually increased from a negative to a positive value.

At the moment of the HO, the pitch angle and a_x of the foot begins to increase as a result of the upward rotation of the heel about the metatarsophalangeal joint occurring while toe contact is maintained. The pitch angle of the shank also begins to increase consistently with the occurrence of knee flexion.

In section IV of Figure 4, the hyperextension of the hip is shown to be reduced due to the upward rotation of the heel, with the tip of the foot being the rotation axis. At this point, the pitch angle (72.2±4.51°) and the a_x (45.4±6.74m/s^2) of the foot, and the pitch angle (49.7±4.43°) of the shank increase to their positive peaks when the knee flexion increases, and the dorsiflexion of the ankle converts to plantar flexion.

3.2 Experiment 2: Stairs ascent

As shown in section I of Figure 5, the hip and knee flexion dramatically increase when the participant's foot is in swing phase while ascending the stairs; in addition, the plantar flexion of the ankle is shifted to dorsiflexion. With these changes, the pitch angle of the foot decreases from a positive peak value (47.6±6.98°) to a negative peak value (-2.13±4.22°) with gradual zero-crossing. The pitch angle of the shank is also decreased from its positive maximum (31.9±9.81°) to its positive minimum value (13.08±3.57°). In regard to acceleration, a_z -in the upward direction- reaches its positive peak (14.52±10.68m/s^2) at the moment of the TO, which then shows gradual change between negative and positive values. a_x -in the walking direction- shows a small positive value (10.48±6.88m/s^2) after the TO, which then decreased lowered down to a negative peak value (-17.86±1.65m/s^2) at the moment of the HS. Thus, the characteristic of the TO movement in ascending the stairs can be interpreted to mean that the velocity involved in the upward direction (v_z) is larger than the velocity involved in the forward walking direction (v_x). The v_x of the foot increases until the middle of the swing phase and decreases before the HS, while the velocity of the heel reaches 0 consistently with the HS. To summarize, the validity of this analysis and decisions made on the moment of the HS can be explained by the result of the pitch angle of the foot being lowered down to its negative peak value.

As shown in sections I to IV of Figure 5, it is confirmed that a_z maintains its positive value during the swing phase in ascending the stairs. As it is close to the HS moment on the upper stair, a_z starts to become a negative value. As mentioned earlier, in the case of walking on flat ground, a_z sharply reverses from a positive to a negative value shortly after the TO because the vertical position of the foot is also lowered shortly after the TO before rising again. That is, from the moment of the TO used for shifting to the HS, a_z shows a tendency to fluctuate between negative and positive values for a short period of time.

As shown in Figure 5, Section II, the stance phase begins at the moment of the HS. From this moment, the hip flexion, knee flexion, and ankle dorsiflexion begin to decrease. As the tip of the toe reaches the stair, the pitch angle of the foot gradually increases to around 0°. The pitch angle of the shank converges to 13°.

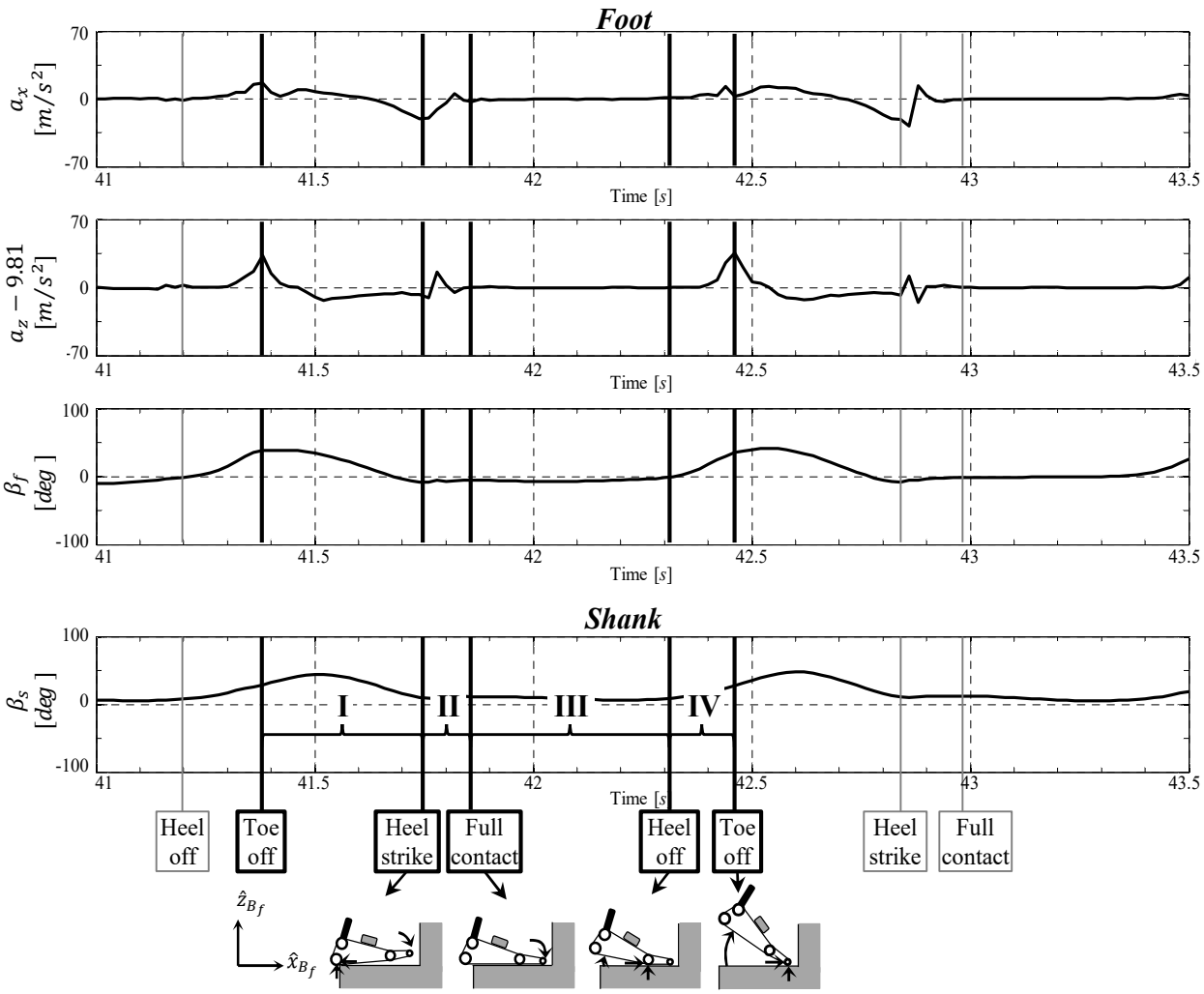

Figure 5. Accelerations and orientation of foot, and orientations of shank in sagittal plane while ascending stairs; time intervals of all sections are as follows: 0.38s for I, 0.04s for II, 0.5s for III, and 0.14s for IV

Also, a_x is sharply lowered to its negative peak (-17.86±1.65m/s^2) with the zero velocity of the heel, because of the friction force between the heel and the upper stair. The a_z is lowered to its negative peak (-6.71±2.72m/s^2), consistent with the fall of foot, which also rose during the swing phase; in addition, a_z sharply increases to a positive value due to the ground reaction force at the moment of contact.

During the FC (Figure 5, Section III), a_x, a_z, and the angle of the foot converge to 0 as the sole is in full contact with the stair. The pitch angle of the shank is maintained at around 13°, because the plantar flexion of the ankle is converted to dorsiflexion, the flexion of hip is also converted to hyperextension, and the flexion of knee is reduced to move forward, similarly to the inverted pendulum motion of the pelvis. At the moment of the HO, pitch angle of foot and shank and a_x start to increase from base. a_z starts to increase from base to positive peak value.

In Figure 5, Section IV, the hip hyperextension is converted to flexion due to the upward rotation of the heel around the rotational

axis of the toe. At this time, the pitch angle (47.6±6.98°) and the a_x (10.48±6.88m/s^2) of the foot, as well as the pitch angle (31.9±9.81°) of the shank, increase to a positive peak when knee flexion increases, and the dorsiflexion of the ankle converts to plantar flexion.

3.3 Experiment 3: Stairs descent

As a result of the video decipher, the toe strike (TS), instead of HS, was observed in the case of descending the stairs. According to Lieberman et al. (2010), the fore-foot strike was reported in the toe-heel-toe running of habitually barefoot runners. In addition, in this research, the fore-foot strike seems to be the same as the toe strike in the case of descending the stairs.

During the swing phase (Figure 6, Section I), hip flexion increases, knee flexion converts to extension, and ankle dorsiflexion converts to plantar flexion. Therefore, the pitch angle of the foot decreases from the first positive peak value (52.3±4.11°) to the second positive peak value (17.30±5.19°), and the pitch angle of the shank decreases from a positive peak value (54.2±3.66°) to a negative peak value (-7.71±2.04°). With regard to acceleration, a_x in the walking direction reached a positive peak value (42.7±5.19m/s^2)

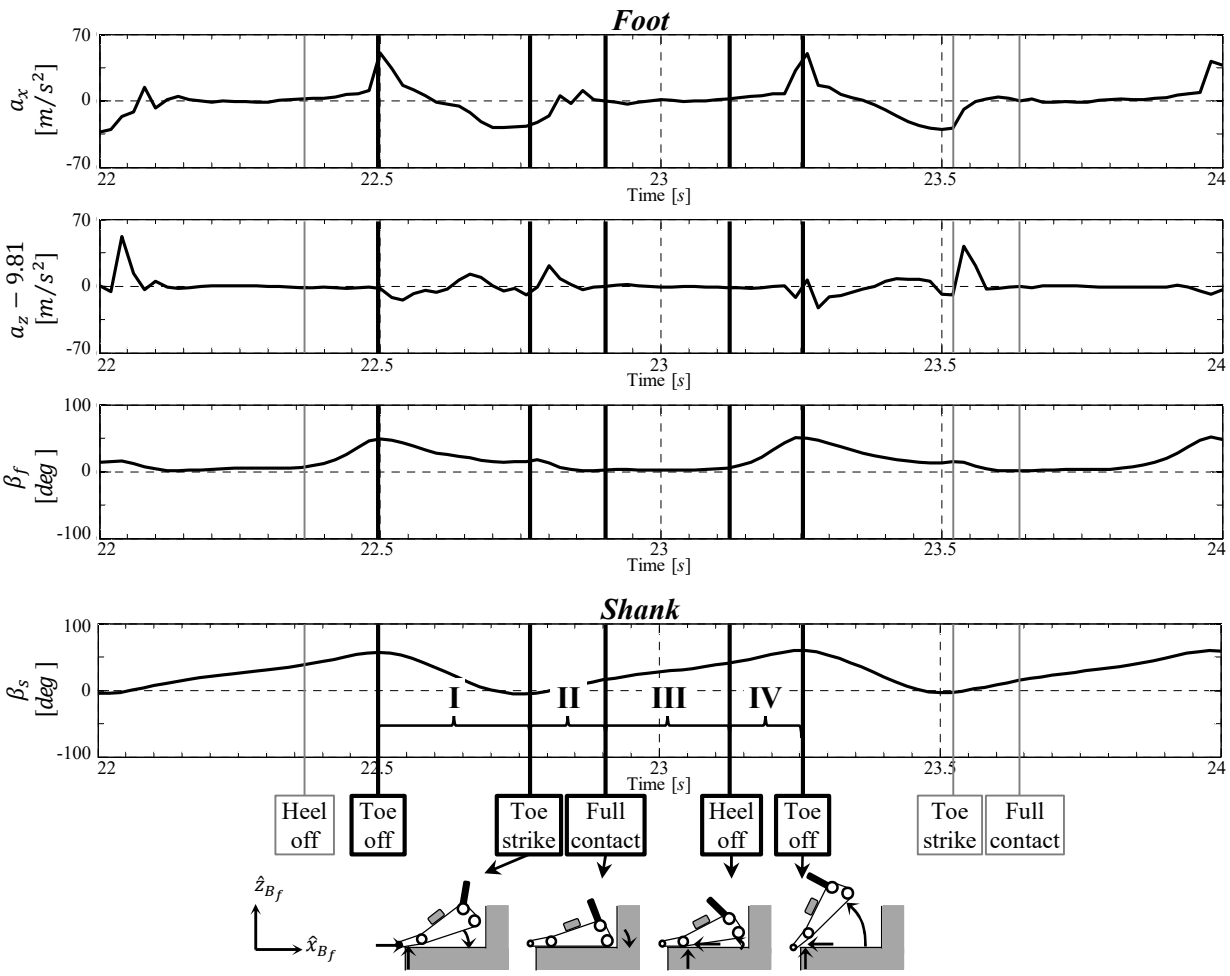

Figure 6. Accelerations and pitch angle of foot, and pitch angle of shank while descending stairs; time intervals of all sections are as follows: 0.36s for I, 0.12s for II, 0.34s for III, and 0.2s for IV

at the moment of the TO and then lowered to a negative peak value (-33.1±6.03m/s^2) at the moment of the TS. The v_x of the foot increases until the middle of the swing phase and decreases before the TS; the velocity of the toe reaches 0, which is consistent with the TS. As the foot approaches the lower stairs during the swing phase, a_z maintains a negative value, but it reverses to a positive value as the downward velocity of the foot decreases. It then falls sharply again to its negative peak as the TC draws close, because the vertical position of the foot lowers for a short period of time after the TO and then rises again. In other words, from the moment of the TO shifting to the TS, it is natural that a_z shows a tendency to fluctuate between negative and positive values for a short period of time. In Figure 6, Section II, the stance phase starts at the moment of the TS. At this time, the hip flexion and the knee flexion increases, and the ankle plantar flexion is converted to dorsiflexion. Because of the downward rotation of the heel around the rotation axis of the toe, the pitch angle of the foot decreased to a second positive peak of almost 0°, while the pitch angle of the shank increased to almost -8°.

In addition, a_x lowers to the negative peak with the zero velocity of the toe, because of the friction force between the toe and the lower stair. The a_z is consistently lowered to the negative peak (-8.47±3.15m/s^2) with the fall of foot, and reaches its positive value as a result of the ground reaction force at the moment of contact. During the FC shown in Figure 6, Section III a_x, a_z and the angle of the foot converge to 0 as the sole comes in full contact with the lower stair. The positive pitch angle of the shank increases, because ankle dorsiflexion and knee flexion become larger and hip flexion becomes smaller in order to move downward with the inverted pendulum motion of the pelvis when the ankle is in an axis of rotation. At the moment of the HO, lower-limb's motion is the same with the case of flat ground.

In Section IV, Figure 6, the hip flexion increases due to the upward rotation of the heel around the toe as a rotation axis. At this moment, the pitch angle (52.3±4.11m/s^2) and a_x (42.7±5.19m/s^2) of the foot and the pitch angle (54.2±3.66m/s^2) of the shank start to sharply increase to their positive peaks as the knee flexion increases and the ankle dorsiflexion decreases.

3.4 Experiment 4: Slope ascent

During the swing phase (Figure 7, Section I), the positive peak value of the pitch angle of the foot (66.8±4.93°) and the shank (35.2±4.97°) starts to decrease to their negative peaks (foot: -23.0±3.49°, shank: -17.62±3.35°). With regard to acceleration, the a_x in the walking direction reaches its positive peak value (44.8±6.58m/s^2) at the moment of the TO and gradually lowers to its negative peak (-30.0±3.48m/s^2) until before the HS.

In Figure 7, Section II, the stance phase starts from the moment of the HS. At this moment, the pitch angle of the foot and the shank is increased from its negative value to around 0°. In the case of ascending a slope, contrary to the other cases, the pitch angle of the foot converges at around 10° (-12.75±2.77°) - the slope of the ground - as it is close to the movement of the FC. Also, a_x is lowered to its negative peak (-30.0±3.48m/s^2). The a_z is lowered to its negative peak (-20.3±4.28m/s^2).

During the FC (Figure 7, Section III), a_x and a_z converge at 0, while the pitch angle converges at the slope of the ground (12.75±2.77°) when the sole is fully in contact with the ground. The pitch angle of the shank changes from a negative to a positive value. At the moment of the HO, the motion of lower-limb is the same with the case of flat ground.

In Figure 7, Section IV, the pitch angle (66.8±4.93°) and the a_x (44.8±6.58m/s^2) of the foot, as well as the pitch angle (35.2±4.97°) of the shank, increase dramatically to their positive peak.

3.5 Experiment 5: Slope descent

During the swing phase (Figure 8, Section I), the pitch angle of the foot (70.13±9.21°) and the shank (60.88±6.46°) are decreased

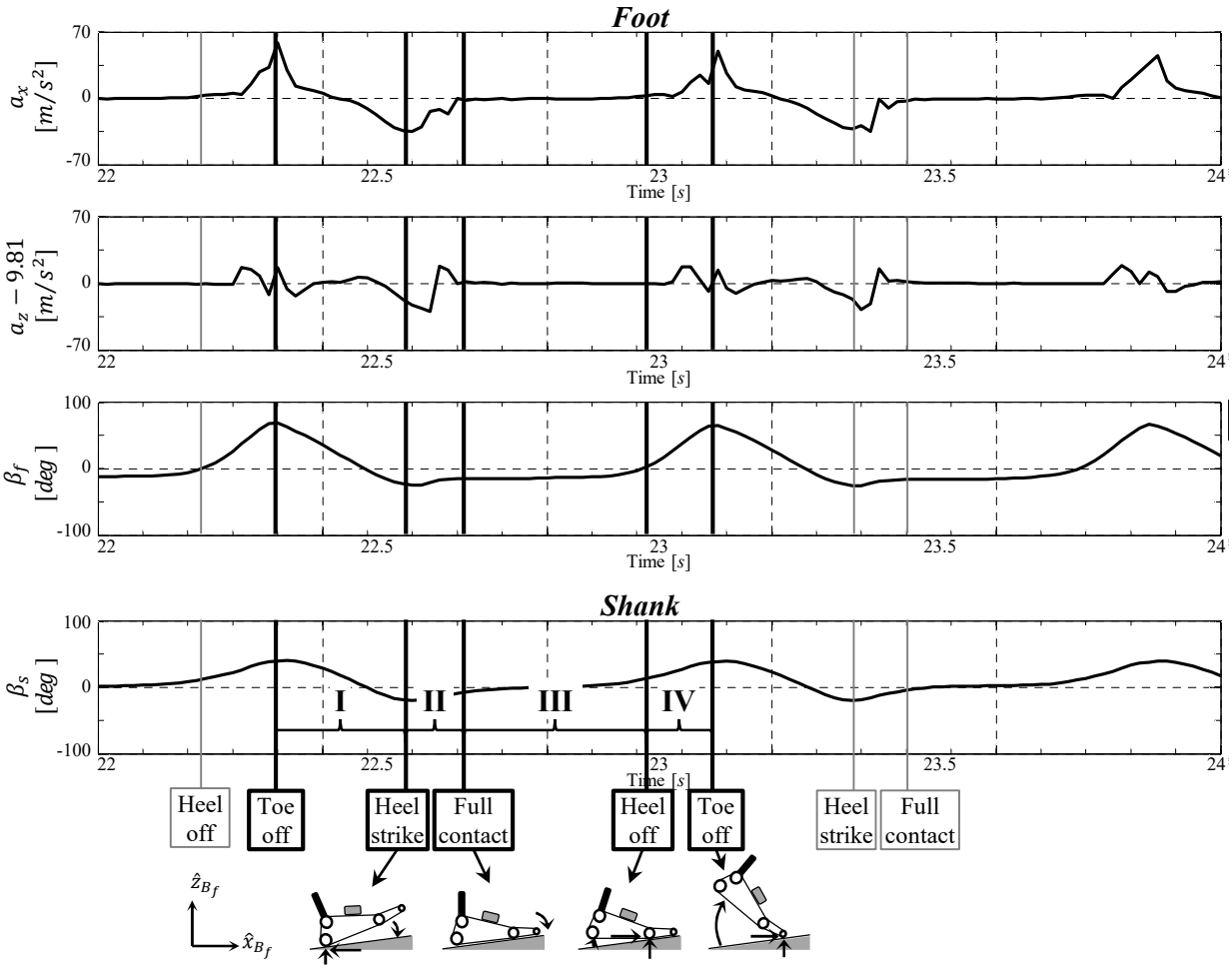

Figure 7. Accelerations and pitch angle of foot, and pitch angle of shank while ascending a slope; time intervals of all section are as follows: 0.38s for I, 0.12s for II, 0.44s for III, and 0.24s for IV

from their positive peaks to negative peaks (foot: -22.2±6.10°, shank: -19.35±3.63°). In regard to acceleration, a_x in walking direction reaches its positive peak value (47.1±7.24m/s^2) at the moment of the TO and lowers to its negative peak (-33.8±3.50m/s^2) immediately the before the HS.

In Figure 8, Section II, the pitch angle of the foot and the shank gradually increase to around 0°. Similar to the slope ascent, the pitch angle of the foot converges at around 10° (7.96±2.36°) - slope of the ground - as it is close to the moment of the FC. Also, a_x is sharply lowered to its negative peak (-33.8±3.50m/s^2) with the zero velocity of the heel. The a_z is lowered to its negative peak (-27.5±3.84m/s^2).

During the FC (Figure 8, Section III), a_x and a_z converge at 0, while the pitch angle converges at the slope of the ground, (7.96±2.36°). The pitch angle of the shank increases from its negative value to a positive value. At the moment of the HO, lower-limb's motion is the same with the case of flat ground.

In Figure 8, Section IV, the pitch angle (70.1±9.21°) and a_x (47.1±7.24m/s^2) of the foot, and the pitch angle (61.9±4.02°) of the

shank, sharply increase to their positive peak.

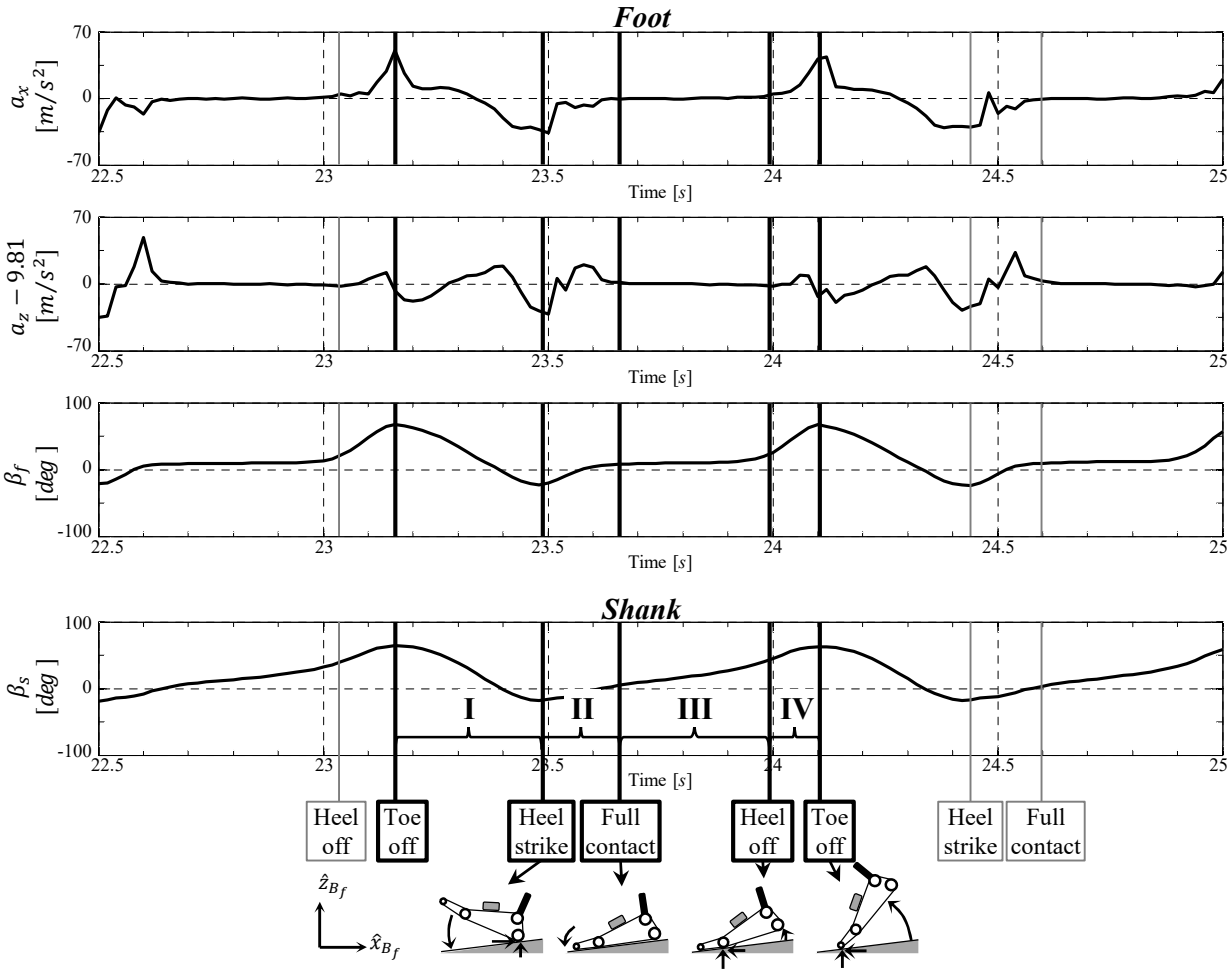

Figure 8. Accelerations and orientations of foot, and orientations of shank in sagittal plane while descending a slope; time intervals of each section is as follows: 0.36s for I, 0.12s for II, 0.3s for III and 0.22s for IV

3.6 Design of FGCD algorithm and issues on IMU sensor installations

Table 2 represents the FGCD threshold ranges of four parameters of a_x, a_z, β_f, and $\dot{\beta}_f$ and their margins for realizing the FGCD algorithm (Figure 10). In the case of the upper threshold values of each parameter, they were determined at the largest value among the values obtained by adding standard deviations to mean values. The positive threshold values are rounded up to the tenth place. In addition, the negative threshold values are also rounded down to the tenth place. However, the lower threshold values of each parameter were determined at the smallest value among the values obtained by subtracting standard deviations from mean values. The positive threshold values are rounded down to the tenth place. Moreover, the negative threshold values are rounded up to the tenth place.

In particular, it is worth noting that the posture of the IMU sensors mounted on the lower-limbs can be slightly changed according to repetitive experiments and changes of the participant or user. In other words, as shown in Figure 9 (a), the orientation of IMU

Table 2. Foot-ground contact detection threshold ranges of four parameters of a_x, a_z, β_f, and $\dot{\beta}_f$ for the four different foot-ground contact phases

Case	Heel strike		Full contact		Heel off		Toe off	
	Min	Max	Min	Max	Min	Max	Min	Max
a_x [m/s^2]	–	-16.3	-1.7	2.3	0.6	4.8	6.7	–
a_z [m/s^2]	–		-1.3	1.4	-1.5	0.7	–	
β_f [deg]	–	20.0	–		–		40.4	–
$\dot{\beta}_f$ [rad/s]	–		-0.4	0.6	1.6	3.8	–	
Margin [%]	20		50		40		20	

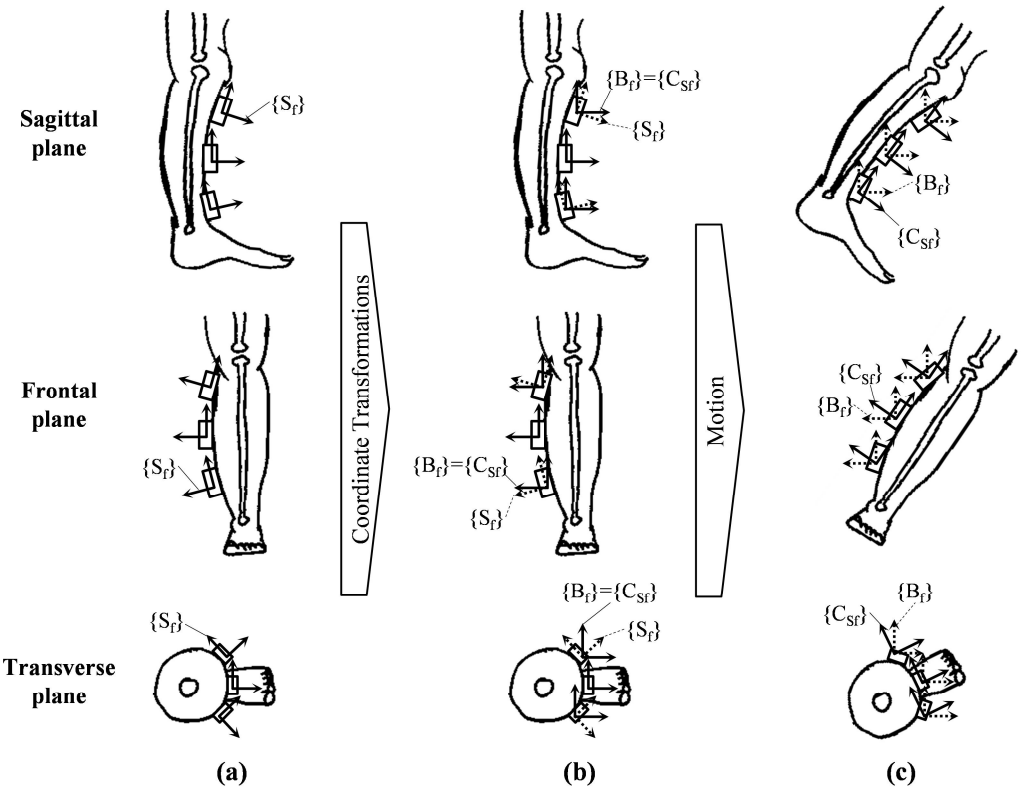

Figure 9. (a) Orientation of sensor fixed-frame {S_f} attached on several position on lower-limb segment when straight aligned, (b) orientations of body fixed frame {B_f} and compensated sensor fixed-frame {C_{Sf}} after post-processing, and (c) orientations of {B_f} and {C_{Sf}} while the body-segment moves

can be different according to installation position although IMU is attached on the same body-segment. That is, a detailed discussion on this sensor installation issue is required because the variation of the posture of the IMU sensors for different participants or users would be a main factor which affects the threshold values in the FGCD algorithm. According to the rigid body dynamics, the variation of the posture of the IMU sensors can affect not the orientation and angular velocity, but the accelerations (Banos et al., 2014). As mentioned earlier, the virtual {B_f} was set on the participant's body as a common reference coordinate frame (Figure 9

(b)). In addition, it allows the coordinate frames of all IMU sensors to be successfully changed to the predetermined $\{B_f\}$. Also, as presented in Figure 9 (b), $\{C_{Sfj}\}$ is created. The orientation of $\{C_{Sfj}\}$ is equal to the orientation of $\{B_f\}$ frame when the posture of participant is straight aligned, and the change of orientation of $\{C_{Sfj}\}$ is the same with the change of orientation of lower-limb segments while the participant is walking. As shown in Figure 9 (c), it can be known that the orientation and angular velocities of $\{C_{Sfj}\}$ expressed in $\{B_f\}$ measured from each IMU sensor are not affected by the variations of sensor installations. However, the acceleration measurement can be affected by the distance of the installed IMU sensor from the center of rotation, unlike the measurement of orientation and angular velocity. This is one of the reasons why the threshold margins are applied to the FGCD threshold values of each contact phase with the consideration on the variations of the installation positions of the sensors; 1) HS: 20%, 2) FC: 50%, 3) HO: 40%, and 4) TO: 20%. The possibility of installing IMU sensors on wearable rigid fixtures will greatly assist to overcome these installation issues, while the flexible fabric straps were used to mount the IMU on the lower-limbs of participants in this research.

Figure 10 represents the developed FGCD algorithm which is possible to detect the four different foot-ground contact phases on the five different walking terrains. As shown in Figure 10, both a_x and β_f at the moment of HS are commonly less than -13.0m/s^2 and 24° in all terrains (Figure 10 HS (a), (c)). In the case of stairs descent, it is confirmed that β_f shows its positive peak value at the moment of TS, while β_f at the other terrains commonly shows negative peak values at the moment of HS moment. Accordingly, β_s is selected as one of the parameters to determine HS and TS in all terrains instead of β_f, because β_s commonly shows negative peak values at the moment of HS and TS moments in all terrains. In addition, $\dot{\beta}_s$ is adopted to find the moment of the peak values of β_s in a numerical way (Figure 10 HS (b)).

In the cases of FC in slope ascent and descent, β_f converges to the angle of inclinations, while β_f on flat ground converges to zero. Accordingly, the rate of β_f, $\dot{\beta}_f$, is selected as one of the parameters to determine FC, regardless of the types of terrain,

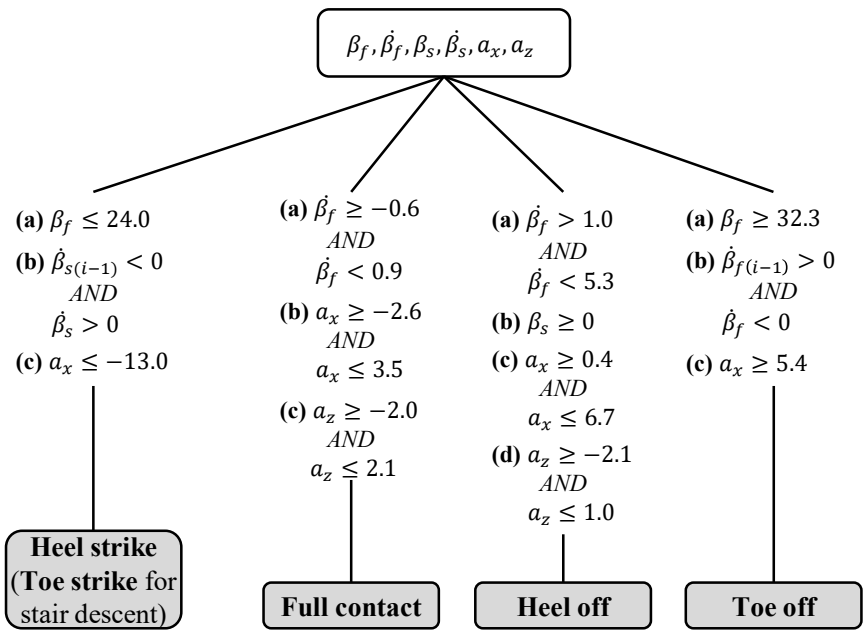

Figure 10. Developed foot-ground contact detection algorithm for possible detection of four different foot-ground contact phases on five different walking terrains; Index *i* represents number of measurements at a sampling rate of 50Hz, β_f represents pitch angle of foot, $\dot{\beta}_f$ represents pitch rate of foot, β_s represents pitch angle of the shank, and $\dot{\beta}_s$ represents rate of pitch and rate of shank

because $\dot{\beta}_f$ commonly converges to zero in all terrains. $\dot{\beta}_f$ ranges from -0.6rad/s to 0.9rad/s (Figure 10 FC (a)). The a_x and a_z do not exactly converge to zero during FC due to the effect of the slight actions of the foot in a state of contact with the foot on the ground. a_x and a_z range from -2.6m/s^2 to 3.5m/s^2 and from -2.0m/s^2 to 2.1m/s^2, respectively (Figure 10 FC (b), (c)).

In the case of HO, $\dot{\beta}_f$, a_x, and a_z increase from 1.0rad/s to 5.3rad/s, from 0.4m/s^2 to 6.7m/s^2, and from -2.1m/s^2 to 1.0m/s^2, respectively (Figure 10 HO (a), (c), (d)), while β_s maintains a positive value (Figure 10 HO (b)). Lastly, in the case of TO, β_f and a_x in all terrains are larger than 32.3° and 5.4m/s^2, respectively (Figure 10 TO (a), (c)). As in the case of HS, $\dot{\beta}_f$ is adopted to find the moment of positive peak values of β_f in a numerical way (Figure 10 TO (b)).

3.7 Experiment 6: Benchmark study on IMU based FGCD algorithm using FSR system

In order to evaluate the performance of the IMU based FGCD algorithm, the moments of HS, FC, HO and TO detected by IMU based FGCD algorithm are compared with benchmark system, FSR-array system. A participant (Age: 26 years, Height: 170cm, Mass: 65kg; Gender: male) is participated for the benchmark study. This participant was not involved in the preceding experiments for developing FGCD algorithm. Informed consent was obtained from the qualified participant prior to his participation in the benchmark study.

Figure 11 shows the β_f output signal of IMU, the moment of HS, FC, HO and TO detected by IMU based FGCD algorithm, and output signal of 4-FSR while walking on the flat ground, as well as up and down a slope and stairs. As shown in Figure 1, FSRs are attached on the heel, MT, toe and ST. Using the output signals from the FSR-array system, each moment of HS, FC, HO, and TO can be correctly detected.

In case of flat ground and slope, as shown in Figure 11 (a) and (b), at the moment of HS detected by IMU based FGCD algorithm, the force of heel starts to increase sharply from base. During FC detected by IMU based FGCD algorithm, the force of heel starts to decrease from maximum value, and the force of MT starts to increase from base. At HO detected by IMU based FGCD algorithm, the force of heel decreases to base, and the forces of toe and ST start to increase from base. Lastly, at the moment of TO detected by IMU based FGCD algorithm, the forces of MT, toe and ST are decreasing rapidly to base. In case of stairs ascent, as shown in Figure 11 (c), at the moment of HS detected by IMU based FGCD algorithm, the forces of heel and MT start to increase. During the early stage of FC detected by IMU based FGCD algorithm, the force of MT shows peak value, and during the late stage of FC detected by IMU based FGCD algorithm, the force of heel shows peak value. At the HO detected by IMU based FGCD algorithm, the force of heel is decreasing to base, the force of MT sharply increases, and the forces of toe and ST also increase. 0.06s before the moment of TO detected by IMU based FGCD algorithm, the forces of toe and ST are decreasing to base. There was a time delay detecting TO while ascending stairs. In case of stairs descent, as shown in Figure 11 (d), at the moment of TS detected by IMU based FGCD algorithm, the force of MT starts to increase sharply from base. During the early stage of FC detected by IMU based FGCD algorithm, the force of MT is decreasing while the force of heel increases to peak, and during the late stage of FC detected by IMU based FGCD algorithm, the force of MT increases drastically again. At the HO detected by IMU based FGCD algorithm, the force of heel is decreased to base, the force of MT increases sharply, and also the forces of toe and ST increase. However, the ST is not on the tread of the stairs sometimes. At that time, the force of ST shows base although it is actual HO. During swing phase, from TO to HS, the forces of heel, MT, toe and ST are base state at all terrain.

As results of FSR based benchmark study, it was confirmed that the IMU based FGCD algorithm can be successfully adapted for walking on flat ground, slope and stairs descent. However, in case of stairs ascent, short time delay of 0.06s was observed when it comes to detecting TO. It can be considered as the moment of zero-crossing of $\dot{\beta}_f$, TO detection condition, is happens about 0.06s after actual TO on the stairs ascent. In order to detect zero-crossing of $\dot{\beta}_f$, FGCD algorithm need to check the moment when the previous sample value of $\dot{\beta}_f$ is positive and the present sample value of $\dot{\beta}_f$ is negative. Therefore, the time delay

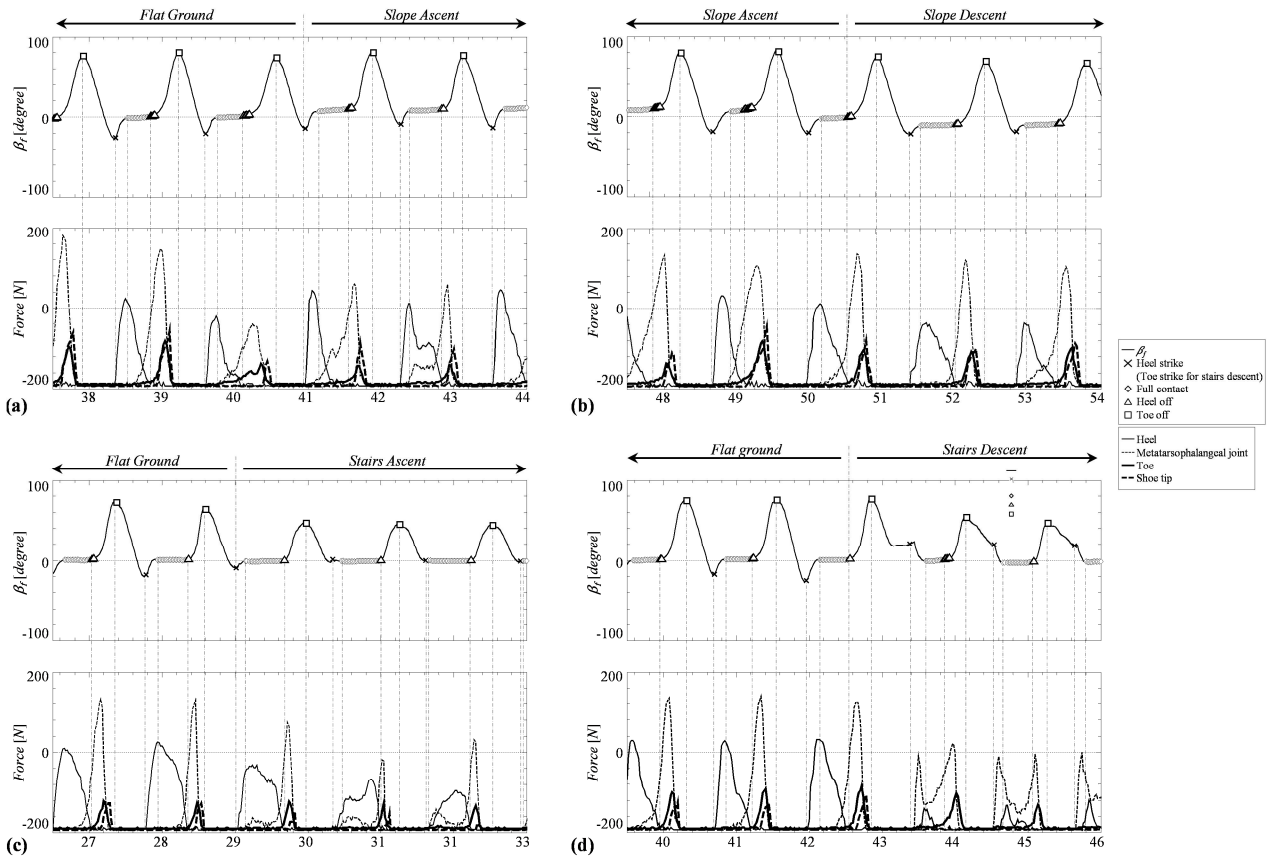

Figure 11. Force sensitive resistor-insole array based benchmark study to estimate performance of foot-ground contact detection algorithm for (a) flat ground and slope ascent, (b) slope ascent and descent, (c) flat ground and stairs ascent, and (d) flat ground and stairs descent

of TO on the stairs ascent can be shorter if the sampling rate of IMU is higher than 50Hz later on. On the other hand, HS, FC and HO was successfully detected.

4. Discussion

Most of the previous works involving the detection of contact between the foot and the ground during gait analysis have used various types of pressure sensors and force sensing resistors (FSR) inside the shoes. However, such methods have various disadvantages, including complex connections between the sensors and the DAQ devices, difficulties in synchronizing with other sensors having different sampling rates, and so on. For these reasons, the ambulatory assessments of the lower limbs for detecting contact between the foot and the ground on various types of terrain are successfully conducted as a form of pre-validation research to help with designing contact detection algorithms using only MTx wireless IMU sensors.

In this study, the experimental environment was limited to three types of terrain: flat ground, a slope, and a set of stairs. Where the slope and the stairs were used, two examples of ascending and descending movements were included. The ambulatory assessments of the lower limbs on each of those terrain types were conducted in order to detect the HS, FC, HO, and TO from a kinematics point of view using only IMU sensors. The result confirmed that the acceleration in the walking and gravitational

directions, and the β_f on all types of terrain included in this study showed similar behaviors. This result can be interpreted to mean that the four steps of contact can be independently detected, the only constraints of which include the ranges, rates of changes, and thresholds of the measurement data.

According to the results of the experiment, it was confirmed that the variations of acceleration in y-direction on all terrains are too small to determine any significant changes. Thus, the gait analysis was mainly conducted in the Sagittal plane, containing the x-axis and z-axis of the three anatomical planes of the human body. Apart from our different frame definition, the results of this analysis are similar to the research results by Bamberg et al. (2008) who used "gait shoe sensors" for gait analysis. In that study, the dorsiflexion and plantar flexion in the ankle, the flexion and extension in the knee, and the flexion and hyperextension in the hip produced motion in the Sagittal plane. The ankle's inversion and eversion and the hip's abduction and adduction are motions in the frontal plane, whereas the hip's inward internal rotation and outward external rotation generate motions in the transverse plane (Adrian and Cooper, 1995). Thus, it is appropriate that the kinematic analysis on the foot and the shank was implemented with respect to the three anatomical planes indicated in the research conducted by Bamberg et al. (2008).

The results concerning cases where flat ground was used, can be summarized as follows: a positive peak of a_x with the TO, a negative peak of a_x and a_z with the HS, the zero-convergence of a_x and a_z during the FC, and an increase of a_x with the HO from a dynamic point of view. These results are similar to those by Bamberg et al. (2008) From the kinematic point of view, positive peaks of β_f and β_s with the TO, and negative peaks of β_f and β_s with the HS were observed.

The differences between walking on level ground and ascending the stairs can be distinguished by the positive peak of not a_x but a_z, with TO, the negative peak of the β_f (which is almost 0), and β_s, which is always larger than 0 in the case of the ascending stairs. a_z of the foot had a positive peak with the TO, while a_x and a_z of the foot had negative peaks with the HS. In addition, a_x and a_z of the foot converge to 0 with the FC, and a_x of the foot gradually increases with the HO. From a kinematic perspective, β_f shows its positive peak with the TO, while showing its negative peak with the HS. The β_s shows a small positive peak with the HS.

The most significant result in the cases involving descending the stairs is the substitution of the HS for the TS, in contrast with walking on the other terrains. β_f shows its second positive peak at the TS. From a dynamic point of view, the results gleaned from the cases where descending the stairs was involved can be summarized as follows. The positive peak of the foot's a_x with TO, the negative peaks of a_x and a_z of the foot with the TS, the convergence of a_x and a_z of the foot toward 0 during the FC, and the gradual increase of a_x of the foot with the HO are observed.

From the kinematic point of view, β_f and β_s show a positive peak with the TO, β_f shows the second positive peak with the TS, and β_s shows a negative peak with the TS.

In the cases involving a slope, the patterns of a_x and a_z of the foot are almost the same as the results from cases involving level ground. The most significant result, however, seems to be the fact that the converged β_f during the FC showed a difference of $12.75\pm2.77^\circ$ for slope ascent and $7.96\pm2.36^\circ$ for descent, caused by the slope of the ground.

In this research, all kinematic and kinetic parameters of the lower-limb in walking on the flat, hill, and stairs are simultaneously measured to examine whether the moments of HS, FC, HO, and TO can be detected with only using these parameters without any force sensors inside of shoes. Consequently, it is successfully discovered that six kinematic and kinetic parameters in each contact moment show common patterns of change regardless of types of walking terrain. Finally, to validate the feasibility of the IMU based FGCD, several repetitive field test were performed with benchmark study system. However, it should be noticed that further studies should be performed to guarantee whether the six kinematic and kinetic parameters proposed in this research are still

available for case including variation of walking velocity, age, and gender.

5. Conclusion

In this study, we've mainly focused on feasibility study for developing IMU based foot-ground contact detection (FGCD) algorithm on the every types of terrain through the lower-limb motion analysis. To realize the IMU based FGCD algorithm, all IMU outputs showing significant changes on the moments of four different foot-ground contacts were fully identified through experiments in five different walking terrains. Finally, it was confirmed that the four different contact phases can be independently detected, regardless of the walking terrains, by only using IMU. In future works, the range of participants should be extended to make the proposed algorithm be robust on variation of age, gender, etc. And also, the supervised learning based on FSR-insole as a reference system will be considered to obtain more concrete and robust model for the proposed FGCD algorithm than current predetermined threshold based decision criterion.

Acknowledgement

This research was supported by the Basic Science Research Program through the National Research Foundation of Korea (NRF) funded by the Ministry of Education (2014R1A1A2055334).

References

Adrian, M. and Cooper, J.M., *The Biomechanics of Human Movement*, Benchmark Press, 1995.

Ahn, S.C., Hwang, S.J., Kang, S.J. and Kim, Y.H., Development and Evaluation of a New Gait Phase Detection System Using FSR Sensors and a Gyrosensor, *Journal of the Korean Society for Precision Engineering*, 21, 196-203, 2004.

Bamberg, S.J.M., Benbasat, A.Y., Scarborough, D.M., Krebs, D.E. and Paradiso, J.A., Gait Analysis Using a Shoe-integrated Wireless Sensor System, *IEEE Transactions on Information Technology in Biomedicine*, 12, 413-423, 2008.

Banos, O., Toth, M.A., Damas, M., Pomares, H. and Rojas, I., Dealing with The Effects of Sensor Displacement in Wearable Activity Recognition, *Sensors*, 14, 9995-10023, 2014.

Benocci, M., Rocchi, L., Farella, E., Chiari, L. and Benini, L., A Wireless System for Gait and Posture Analysis Based on Pressure Insoles and Inertial Measurement Units, *Proceeding of the 3rd International Conference on Pervasive Computing Technologies for Healthcare*, (pp. 1-6), London, 2009.

Bergmann, J.H.M., Mayagoitia, R.E. and Smith, I.C.H., A Novel Method for Determining Ground-referenced Contacts During Stair Ascent: Comparing Relative Hip Position to Quiet Standing Hip Height, *Gait & Posture*, 31(2), 164-168, 2010.

Chen, M., Yan, J. and Xu, Y., Gait Pattern Classification with Integrated Shoes, *Proceedings of the annual Conference on Intelligent Robots and Systems*, (pp. 833-839), St. Louis, 2009.

Choi, J.H. and Hong, W.H., A Suggestion on a New Correction Coefficient for SIMULEX Egress Model to Predict Agent's Stair Slope Travel Time in a High-rise Building, *Journal of the Architectural Institute of Korea: Planning & Design*, 29, 285-292, 2013.

Dadashi, F., Mariani, B., Rochat, S., Büla, C.J., Santos-Eggimann, B. and Aminian, K., Gait and Foot Clearance Parameters Obtained

Using Shoe-worn Inertial Sensors in a Large-population Sample of Older Adults, *Sensors*, 14, 443-457, 2014.

D'Attanasio Honiger, S., Micallef, J.P., Peruchon, E., Guiraud, D. and Rabischong, P., A Robust, Economic and Ergonomic Sensor Device for Gate Phase Detection for an Implanted FES System, *Proceeding of the annual Conference on International Functional Electrical Stimulation Society*, Cleveland, 2001.

Eng, J.J., and Winter, D.A., Kinetic Analysis of the Lower Limbs During Walking: What Information Can be Gained From a Three-dimensional Model?, *Journal of biomechanics*, 28, 753-758, 1995.

Ferrari, A., Ginis, P., Hardegger, M., Casamassima, F., Rocchi, L. and Chiari, L., A Mobile Kalman-Filter Based Solution for the Real-Time Estimation of Spatio-Temporal Gait Parameters, *Neural Systems and Rehabilitation Engineering, IEEE Transactions On*, (99), 2015.

Hogg, R.W., Rankin, A.L., Roumeliotis, S.I., McHenry, M.C., Helmick, D.M., Bergh, C.F. and Matthies, L., Algorithms and Sensors for Small Robot Path Following, *Proceeding of Annual Conference for the Society of IEEE International Conference on Robotics and Automation (ICRA)*, Washington, 2002.

John, J.C., *Introduction to Robotics*, Pearson Prentice Hall, 2005.

Kim, M. and Lee, D., Development of an IMU based foot-ground contact detection (FGCD) algorithm, *Ergonomics*, (just-accepted), 1-23, 2016.

Li, Y., Luo, X., Ren, X.T. and Wang, J.J., A Robust Humanoid Robot Navigation Algorithm with ZUPT, *Proceeding of Annual International Conference on Mechatronics and Automation*, Sichuan Chengdu, 2012.

Li, Y. and Wang, J.J., A Robust Pedestrian Navigation Algorithm with Low Cost IMU, *Proceeding of Annual International Conference on Indoor Positioning and Indoor Navigation (IPIN)*, Sydney, 2012.

Lieberman, D.E., Venkadesan, M., Werbel, W.A., Daoud, A.I., D'Andrea, S., Davis, I.S., Mang'Eni, O.R. and Pitsiladis, Y., Foot Strike Patterns and Collision Forces in Habitually Barefoot Versus Shod Runners, *Nature*, 463, 531-535, 2010.

Morioka, K., Lee, J.H. and Hashimoto, H., Human-following Mobile Robot in a Distributed Intelligent Sensor Network, *Industrial Electronics, IEEE Transactions On*, 51, 229-237, 2004.

Ng, T.C., Ibañez-Guzmán, J., Shen, J., Gong, Z., Wang, H. and Cheng, C., Vehicle Following with Obstacle Avoidance Capabilities in Natural Environments, *Proceeding of Annual International Conference on Robotics and Automation (ICRA)*, New Orleans, 2004.

Nistler, J.R. and Selekwa, M.F., Gravity Compensation in Accelerometer Measurements for Robot Navigation on Inclined Surfaces, *Procedia Computer Science*, 6, 413-418, 2011.

Pappas, I.P., Keller, T., Mangold, S., Popovic, M.R., Dietz, V. and Morari, M., A Reliable Gyroscope-based Gait-phase Detection Sensor Embedded in a Shoe Insole, *IEEE Sensors Journal*, 4, 268-274, 2004.

Pappas, I.P., Popovic, M.R., Keller, T., Dietz, V. and Morari, M., A Reliable Gait Phase Detection System, *Neural Systems and Rehabilitation Engineering, IEEE Transactions On*, 9, 113-125, 2001.

Park, S.J., Lee, J.S., Gang, D.H., Jung, E.H., Jung, H.J. and Park, S.B., Research on Walking Speed and Stride According to Age, *Proceeding of Annual Conference on The Ergonomics Society of Korea*, Busan, 2007.

Salarian, A., Burkhard, P.R., Vingerhoets, F.J., Jolles, B.M. and Aminian, K., A Novel Approach to Reducing Number of Sensing Units for Wearable Gait Analysis Systems, *Biomedical Engineering, IEEE Transactions On*, 60, 72-77, 2013.

Seco, F., Prieto, C. and Guevara, J., A Comparison of Pedestrian Dead-reckoning Algorithms Using a Low-cost MEMS IMU, *Proceeding of the Annual Conference on the Society of IEEE International Symposium on Intelligent Signal Processing*, Budapest, 2009.

Shimizu, T., Awai, M., Yamashita, A. and Kaneko, T., Mobile Robot System Realizing Human Following and Autonomous Returning Using Laser Range Finder and Camera. *Proceeding of the Annual Conference on the Society of Fontiers of Computer Vision (FCV)*, Kawasaki, 2012.

Yuan, Q. and Chen, I., Human Velocity and Dynamic Behavior Tracking Method for Inertial Capture System, *Sensors and Actuators A: Physical*, 183, 123-131, 2012.

Yuan, Q. and Chen, I., Localization and Velocity Tracking of Human via 3 IMU Sensors, *Sensors and Actuators A: Physical*, 212, 25-33, 2014.

Author listings

Myeongkyu Kim: mk.kim0977@gmail.com
Highest degree: M.S., Department of Mechanical Engineering, Soongsil University
Position title: Researcher, Department of Mechanical Engineering, Soongsil University
Areas of interest: Applied Ergonomics, Robotics, Human-Robot Interface

Donghun Lee: dhlee04@ssu.ac.kr
Highest degree: PhD, Department of Mechanical & Aerospace Engineering, Seoul National University
Position title: Professor, Department of Mechanical Engineering, Soongsil University
Areas of interest: Applied ergonomics, Autonomous mobile robots, Human-Robot Interactions, Redundant parallel kinematic mechanisms